

## Exact Hydrodynamic Description of Active Lattice Gases

Mourtaza Kourbane-Houssene,<sup>1</sup> Clément Erignoux,<sup>2</sup> Thierry Bodineau,<sup>3</sup> and Julien Tailleur<sup>1</sup>

<sup>1</sup>*Université Paris Diderot, Sorbonne Paris Cité, MSC, UMR 7057 CNRS, 75205 Paris, France*

<sup>2</sup>*Instituto de Matemática Pura e Aplicada, CEP 22460-320, Rio de Janeiro, Brazil*

<sup>3</sup>*CMAP, Ecole polytechnique, CNRS, Université Paris-Saclay, 91128 Palaiseau, France*

 (Received 26 January 2018; revised manuscript received 23 April 2018; published 29 June 2018)

We introduce lattice gas models of active matter systems whose coarse-grained “hydrodynamic” description can be derived exactly. We illustrate our approach by considering two systems exhibiting two of the most studied collective behaviors in active matter: the motility-induced phase separation and the transition to collective motion. In both cases, we derive coupled partial differential equations describing the dynamics of the local density and polarization fields and show how they quantitatively predict the emerging properties of the macroscopic lattice gases.

DOI: [10.1103/PhysRevLett.120.268003](https://doi.org/10.1103/PhysRevLett.120.268003)

Active matter systems are intrinsically out of thermal equilibrium due to the dissipation of energy at the microscopic scales to produce motion [1–4]. The resulting non-Brownian random walks endow these systems with a rich phenomenology, from the long-range order observed in 2D assemblies of self-propelled particles [5–8] to the spatio-temporal chaos of dense assemblies of nematic particles [9,10] through the enhanced clustering resulting from the interplay of repulsive forces and self-propulsion [11–13].

The toolbox of equilibrium statistical mechanics cannot be used *a priori* to describe such nonthermal systems and one has to rely on dynamical studies, even to characterize systems in a steady state. When an effective detailed balance with respect to a non-Boltzmann distribution is (partially) restored [14–16], this can only be established after a complex case-by-case study of otherwise analytically untractable dynamics. Numerical simulations have thus become a prominent tool to study active matter, and progress is often hindered by strong finite-size effects [17]. In such contexts, exact results derived on simple model systems can offer much needed guiding principles. Whereas this has frequently been true outside equilibrium, for instance, to characterize dynamical phase transitions [18], little success has been achieved along these lines for active matter systems. In particular, the derivation of coarse-grained descriptions of active systems has attracted a lot of interest over the past decades [19–31], but the complexity of the underlying microscopic models has prevented the derivation of exact results outside the mean-field regime [32,33].

In this Letter, following the recent interest for lattice models of active particles [27,31,34–40], we introduce new active lattice gas models whose large-scale physics can be described exactly. We build on recent developments in the mathematical-physics literature to derive exact coarse-grained “hydrodynamic” descriptions of lattice gases [41–44]. For illustration purposes, we focus on two of the

most studied emergent behaviors in active systems: the motility-induced phase separation (MIPS) [11,15,45] and the transition to collective motion [5,17,46], but the approach we present here can be extended beyond these cases. For both systems, we single out the relevant coarse-grained fields and construct their exact dynamics. This allows us both to simulate efficiently their large-scale behaviors as well as analytically study their instabilities and the corresponding phase diagrams.

We first consider a microscopic lattice gas that exhibit MIPS.  $N$  particles evolve on a discrete ring of  $\alpha L$  sites. There are two types of particles and each site is occupied by at most one particle so that a configuration can be represented using occupation numbers  $\sigma_i$  at site  $i$  with values in  $\{-1, 0, 1\}$ . To model self-propulsion, we endow the  $+$  particles with a weak drift to the right and the  $-$  particles with a weak drift to the left, in addition to a symmetric diffusive motion. Furthermore, a particle can tumble and change sign at a fixed rate. More precisely, the dynamics combine three mechanisms: (1.1) For each bond  $(i, i + 1)$ ,  $\sigma_i$  and  $\sigma_{i+1}$  are exchanged at rate  $D$ . (1.2) For each bond  $(i, i + 1)$ , a  $+$  particle in  $i$  jumps to  $i + 1$  if  $\sigma_{i+1} = 0$  or a particle in  $i + 1$  jumps to  $i$  if  $\sigma_i = 0$ , at rate  $\lambda/L$ . (1.3) Particles switch sign at rate  $\gamma/L^2$ .

As we show below, each mechanism will play a specific role in the coarse-grained equations. The total number of particles is  $N \equiv \rho_0 \alpha L$ , where  $\rho_0 \in [0, 1]$  stands for the mean density. The system remains homogeneous for small  $\rho_0$  or  $\lambda$ , whereas the homogeneous phases become unstable for large densities and drift. The previous dynamics can be generalized to higher dimensions. We show in Fig. 1 the result of 2D numerical simulations leading to the coexistence between dilute and dense phases typical of MIPS. Depending on whether the 2D case is built solely with a left-right bias or whether one considers biases along each of the four directions, we observe different symmetries for the coexistence phases.

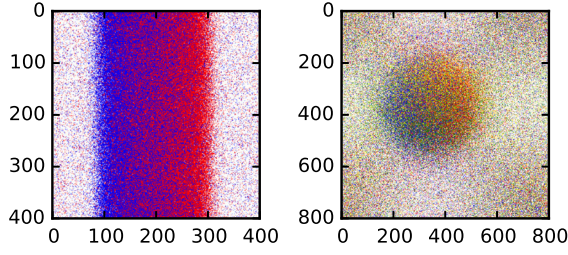


FIG. 1. Snapshots of microscopic simulations of dynamics 1.1–1.3 in 2D showing MIPS for lattices of  $\alpha L \times \alpha L$  sites, with  $L = 100$ . The symmetry of the dense phase depends whether particles are biased only along  $\hat{x}$  (left,  $\alpha = 4$ ,  $\rho_0 = 0.65$ ) or can point along the four lattice bonds (right,  $\alpha = 8$ ,  $\rho_0 = 0.63$ ). The color of a site gives the direction of a particle: blue for right, green for up, red for left, yellow for down. Simulation parameters:  $D = 1$ ,  $\gamma = 10$ ,  $\lambda = 40$ .

To account for this phenomenology, one needs to characterize the evolution of the local density of particles. Let  $\sigma_i^\pm(t)$  equal 1 when a particle with sign  $\pm 1$  is present at site  $i$  and time  $t$  and 0 otherwise, then

$$\begin{aligned} \partial_t \langle \sigma_i^+ \rangle &= D[\langle \sigma_{i+1}^+ \rangle + \langle \sigma_{i-1}^+ \rangle - 2\langle \sigma_i^+ \rangle] - \frac{\gamma}{L^2} [\langle \sigma_i^+ \rangle - \langle \sigma_i^- \rangle] \\ &\quad + \frac{\lambda}{L} [\langle \sigma_{i-1}^+ (1 - |\sigma_i|) \rangle - \langle \sigma_i^+ (1 - |\sigma_{i+1}|) \rangle]. \end{aligned} \quad (1)$$

These equations are, however, not closed, since the evolution of  $\langle \sigma_i^\pm(t) \rangle$  involves the correlator  $\langle \sigma_i^\pm(t) \sigma_{i+1}(t) \rangle$ .

A closed, explicit description of the dynamics can, however, be achieved at the macroscopic level. Indeed, following [41–44], we chose the three processes above to occur with rates scaling with  $L$  in such a way that they all contribute equally to a coarse-grained regime obtained by a diffusive rescaling of space and time:  $x = i/L$  and  $\tau = t/L^2$ . Indeed, the first dynamical rule leads to the diffusion of the particles: if one follows the particles without their signs, the exchange dynamics 1.1 amount to a symmetric simple exclusion process. This first rule makes particles travel a distance  $\Delta i \sim L$  on a time  $\delta t \sim L^2$  and hence at a macroscopic scale  $\Delta x \sim 1$  for  $\Delta \tau \sim 1$ . The second rule applies at a reduced rate  $\lambda/L$ , but provides a systematic drift to the left or to the right depending on the particle type. Similarly, in a time  $L^2$ , this leads to a displacement of order  $L$ . Finally, at an even more reduced rate  $\gamma/L^2$ , the particle type changes, which boils down to saying that a particle changes direction once in a macroscopic unit of time. This occurs sufficiently rarely so that the drift has a macroscopic effect between two updates.

To derive the dynamical behavior of the system in the large  $L$  limit, we introduce the macroscopic densities as

$$\rho_L^\pm(x, \tau) = \frac{1}{2L^\delta} \sum_{|i-Lx| \leq L^\delta} \sigma_i^\pm(\tau L^2), \quad (2)$$

where the coarse graining scale is determined by the parameter  $\delta \in (0, 1)$  [47]. Our choice of the microscopic

system size  $\alpha L$  depends on two parameters:  $L^{-1}$  plays the role of a microscopic mesh; it vanishes in the  $L \rightarrow \infty$  limit in which  $\alpha$  then controls the rescaled system size  $x \in [0, \alpha]$ . The macroscopic equations for the densities  $\rho^\pm \equiv \lim_{L \rightarrow \infty} \rho_L^\pm$ , starting from a smooth initial condition, can then be derived exactly as

$$\partial_\tau \rho^+ = D \partial_x^2 \rho^+ - \lambda \partial_x [\rho^+ (1 - \rho)] - \gamma (\rho^+ - \rho^-), \quad (3)$$

$$\partial_\tau \rho^- = D \partial_x^2 \rho^- + \lambda \partial_x [\rho^- (1 - \rho)] + \gamma (\rho^+ - \rho^-), \quad (4)$$

where the total density is  $\rho = \rho^+ + \rho^-$ . Following standard notations [48], we refer to Eqs. (3) and (4) as the hydrodynamic description of our microscopic model [49]. The mathematical method to rigorously derive these hydrodynamic equations has been initiated in [41,42] and we refer to [44] for a detailed implementation. We will explain below the underlying principles. Intuitively, Eq. (3) can be deduced from the microscopic equation (1) by first replacing the discrete differences by derivatives. Justifying the forms of the nonlinear advection terms requires one to close the two-point correlations in (1). Even though on a macroscopic scale the three mechanisms of the dynamics compete at equal footing, the first one dominates locally as it occurs much more frequently. Thus, in the large  $L$  limit, it can be shown that the local correlations are controlled by the diffusive part. The invariant measures of the dynamics reduced to the diffusive part are product Bernoulli measures indexed by two parameters, which prescribe the local densities of  $\pm$  particles. Thus, at any time, the local statistics of the full dynamics are determined by a product of Bernoulli measures parametrized by the local densities (2); this is sometimes referred to as “local equilibrium” [48]. The approximation by these local measures is valid beyond the expectation of the correlations and applies at the level of sample paths so that local averages as in (2) converge with high probability to the solution of the hydrodynamic equations (3) and (4). Note that the hydrodynamic equations directly extend to higher dimensions. We compare in Fig. 2 simulations of the microscopic and macroscopic dynamics for the 1D case. A perfect agreement between the two dynamics is observed on their way to phase coexistence.

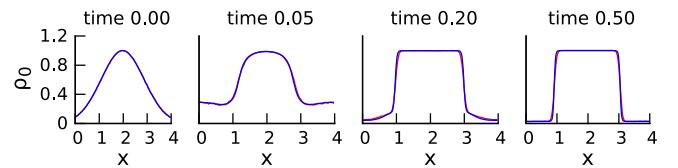


FIG. 2. Successive snapshots leading to phase coexistence in 1D: the microscopic (red) and macroscopic (blue) simulations agree quantitatively. Simulation parameters:  $D = 1$ ,  $\lambda = 5$ ,  $\gamma = 0.1$ ,  $\rho_0 = 0.75$ ,  $\alpha = 4$ . Microscopic simulations: continuous time simulations of dynamics 1.1–1.3 with  $L = 1000$ , averaged over 200 runs. Macroscopic simulations: semispectral method with  $n = 50$  modes and semi-implicit Euler time stepping ( $dt = 10^{-4}$ ).

To analyze the emerging behaviors predicted by (3) and (4), we first introduce an unnormalized polarization field  $m = \rho^+ - \rho^-$ . The dynamics can then be reduced to a dimensionless form using  $x \rightarrow \sqrt{(D/\gamma)}x$  and  $t \rightarrow t/\gamma$ , so that  $x \in [0; \alpha\sqrt{(\gamma/D)}]$ . In this system of units, the evolution equation reads

$$\partial_t \rho = \Delta \rho - \text{Pe} \nabla [m(1 - \rho)], \quad (5)$$

$$\partial_t m = \Delta m - \text{Pe} \nabla [\rho(1 - \rho)] - 2m, \quad (6)$$

with  $\text{Pe} = (\lambda/\sqrt{D\gamma})$ . Equations (5) and (6) show that the system is fully characterized by two control parameters: the density  $\rho_0 = N/L$  and the Péclet number  $\text{Pe}$ . The latter compares the length traveled between two successive tumbles thanks to the drift  $\lambda/\gamma$  to the one resulting from the diffusive dynamics  $\sqrt{D/\gamma}$ . For small Péclet numbers, the diffusion dominates and the effect of self-propulsion is negligible. Conversely, the effect of activity gets more and more pronounced as  $\text{Pe}$  increases.

The homogeneous solutions of Eqs. (5) and (6),  $\rho(x, t) = \rho_0$  and  $m(x, t) = 0$ , are linearly unstable when

$$\text{Pe}^2(1 - \rho_0)(2\rho_0 - 1) > 2. \quad (7)$$

For any  $\text{Pe}$  larger than a critical value  $\text{Pe}^c = 4$ , the system is thus linearly unstable for  $\rho_0 \in [\rho_l^s, \rho_h^s]$ , with  $\rho_{l,h}^s = \frac{3}{4} \pm \frac{1}{4} \sqrt{1 - (16/\text{Pe})}$ . This defines the spinodal region of the system. Note that this is a large wavelength instability, observed only for macroscopic system size  $L_\alpha \equiv \alpha\sqrt{(\gamma/D)} > (2\pi/\sqrt{\text{Pe}^2(1 - \rho_0)(2\rho_0 - 1) - 2})$ . We now turn to the computation of the coexisting densities.

Hydrodynamic descriptions can sometimes be used to compute the nonlinear profiles connecting coexisting phases [50–52]. Here, we generalize the method introduced in [53,54] to compute the binodal curves. For simplicity, we consider the 2D case with left-right bias, in which the interfaces between the phases are flat and along  $\hat{y}$ . We consider fully phase-separated profiles and use Eqs. (5) and (6) to construct a domain-wall solution, describing the evolution of the density and magnetization fields through an interface. By symmetry, the steady state has a vanishing density flux so that Eq. (5) leads to  $m = (1/\text{Pe})(\nabla\rho/1 - \rho)$ . Equation (6) then reads  $\partial_x g = 0$ , with

$$g \equiv g_0(\rho) + \Lambda(\rho)(\partial_x \rho)^2 - \kappa(\rho)\partial_{xx}\rho, \quad (8)$$

where  $\Lambda(\rho)^{-1} = -\text{Pe}(1 - \rho)^2$ ,  $\kappa(\rho)^{-1} = \text{Pe}(1 - \rho)$ , and  $g_0(\rho) = \text{Pe}\rho(1 - \rho) - 2\log(1 - \rho)/\text{Pe}$ . Since the density is homogeneous in the gas and liquid phases, one gets a first relationship between the coexisting densities

$$g_0(\rho_g) = g_0(\rho_\ell) \equiv \bar{g}(\text{Pe}). \quad (9)$$

To determine  $\rho_\ell$  and  $\rho_g$ , we need to complement (9) by a second equation. Following [53,54], we define  $I = \int_{x_\ell}^{x_g} g \partial_x R(\rho) dx$ , where  $R$  is a monotonically increasing function of  $\rho$ . Using that  $g(x) = \bar{g}$ ,  $I$  can be readily computed as

$$I = \bar{g}[R(\rho_\ell) - R(\rho_g)]. \quad (10)$$

Computing  $I$  using the explicit form of  $g$  [Eq. (8)] is difficult because of the gradient terms. For the specific function  $R(\rho)$  such that  $R''\kappa = -(2\Lambda + \kappa')R'$ , this can be done explicitly, leading to

$$I = \phi(R_\ell) - \phi(R_g), \quad (11)$$

where  $(d\phi(R)/dR) = g_0(\rho)$ . Equations (10) and (11) then enforce the equality of  $h_0 \equiv \phi'(R)R - \phi(R)$  between the two phases. The function  $R$  and  $\phi$  can be computed explicitly as

$$\begin{aligned} R(\rho) &= \log(1 - \rho); \\ \phi(R) &= \text{Pe} \left( 1 - \frac{e^R}{2} \right) e^R - \frac{R^2}{\text{Pe}}. \end{aligned} \quad (12)$$

The binodals are then obtained from the equality of  $g_0$  and  $h_0$  between the two phases, which amounts to a common tangent construction on  $\phi(R)$ . The resulting phase diagram is shown in Fig. 3. It shows perfect agreement with simulations of the hydrodynamic equations and of the microscopic model in 2D. As far as we are aware, this is the first microscopic model for which the hydrodynamic description and the phase diagram of the MIPS can be derived exactly.

We now turn to the phase transition leading to collective motion, which is probably the most studied emerging behavior in active matter [1,5–8,17,27,46]. Following the strategy laid out in the first part of this Letter, we introduce a microscopic model of polar aligning active particles and derive its hydrodynamic limit exactly. For simplicity, we first describe the model in one dimension.  $N$  particles

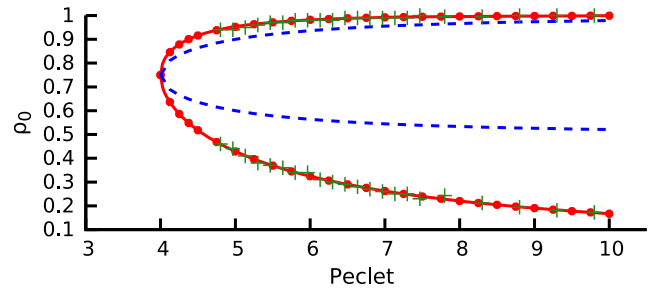


FIG. 3. Phase diagram of the MIPS observed for dynamics 1.1–1.3. For each Péclet number, the coexisting densities are computed analytically (red line) by simulating the microscopic process (green crosses) and by numerically solving the macroscopic equations (red crosses). The analytic predictions for the spinodals are shown in blue.

evolve on a discrete ring of  $\alpha L$  sites. Each particle is described by 2 degrees of freedom: its position  $i \in \{1, \dots, L\}$  and its orientation, noted  $\pm$  in 1D. We call  $\eta_i = (\eta_i^+, \eta_i^-) \in \mathbb{N}^2$  the number of particles of each type on site  $i$ . The dynamics of a  $\pm$  particle is given by the three following processes: (2.1) symmetric hops with rate  $2D$ , (2.2) jumps from site  $i$  to  $i \pm 1$  with rate  $(\lambda/L)$ , and (2.3) flips into a  $\mp$  particle with rate  $(1/L^2)c_i^\pm(\eta_i^+, \eta_i^-)$ , where we choose  $c^\pm$  to produce a polar alignment

$$c_i^\pm(\eta_i^+, \eta_i^-) = \exp[\mp \beta(\eta_i^+ - \eta_i^-)]. \quad (13)$$

Note the lack of exclusion in this process.

We consider again a diffusive rescaling of time and space to obtain the exact hydrodynamic equations

$$\partial_t \rho^+ = D\Delta \rho^+ + \lambda \nabla \rho^+ - F(\rho^+, \rho^-), \quad (14)$$

$$\partial_t \rho^- = D\Delta \rho^- - \lambda \nabla \rho^- + F(\rho^+, \rho^-), \quad (15)$$

where  $F$  is the average of  $n^+ c^+(n_i^+, n_i^-) - n^- c^-(n_i^+, n_i^-)$  with respect to the local Poisson measure

$$\nu_{\rho^+, \rho^-}(n_i^+, n_i^-) = e^{-\rho^+ - \rho^-} \frac{(\rho^+)^{n_i^+} (\rho^-)^{n_i^-}}{(n_i^+)! (n_i^-)!}. \quad (16)$$

Again, while the dynamical rules 2.1–2.3 all contribute equally in the hydrodynamic scaling, the symmetric random walk equilibrates much faster on the microscopic mesh scale. The averages of the nonlinear contributions due to the flipping rules are thus computed with respect to local Poisson measures, which are the steady-state measures of the symmetric random walk, conditioned to produce the correct mean local densities of  $+$  and  $-$  particles. Finally, the hydrodynamic equations (14) and (15) can be rewritten in the more familiar form

$$\partial_t \rho = D\Delta \rho + \lambda \nabla m, \quad (17)$$

$$\partial_t m = D\Delta m + \lambda \nabla \rho - 2\tilde{F}(m, \rho), \quad (18)$$

where

$$\tilde{F} = (m \cosh[m \sinh(\beta)] - \rho \sinh[m \sinh(\beta)]) \times e^{-\beta + \rho \cosh(\beta) - \rho} \quad (19)$$

is deduced from  $F$  by a change of variables and is *not* equal to the mean-field expectation of  $n^+ c^+ - n^- c^-$ .

Simulations of the microscopic model and its hydrodynamic description confirm the presence of a transition to collective motion: at large “temperature”  $T \equiv \beta^{-1}$  and low density  $\rho_0 = N/V$ , the system is in a homogeneous disordered ( $m = 0$ ) “gas” phase. At low noise and large density, the system is in a homogeneous ordered ( $m \neq 0$ )

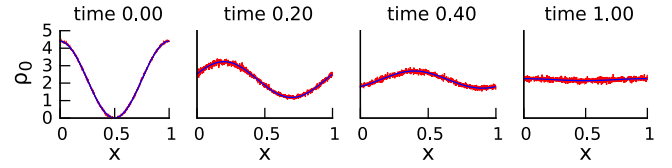


FIG. 4. Successive snapshots of 1D simulations of the dynamics 2.1–2.3 and of the hydrodynamic equations (17) and (18). The system is in the ordered phase and the initial condition is fully ordered with  $\rho(x, 0) = \rho_0[1 + \cos(2\pi x)]$ . Microscopic simulations: the density profiles are averaged over 300 simulations of the dynamics 2.1–2.3 on a lattice of  $L = 1000$  sites ( $\alpha = 1$ ). Macroscopic simulations: pseudospectral simulations with 50 Fourier modes and a semi-implicit time stepping with  $dt = 10^{-4}$ . Physical parameters:  $D = 0.5$ ,  $\lambda = 4$ ,  $\beta = 0.8$ .

“liquid” phase; there, particles hop, on average, in the same direction, hence leading to “collective motion.” These homogeneous phases are separated by a coexistence region in which a dilute disordered gas of density  $\rho_g(T)$  coexists with a dense liquid phase of density  $\rho_\ell(T)$ . A perfect agreement between simulations of the microscopic model and of its hydrodynamic description is shown in Fig. 4 where the relaxation of a perturbation towards an ordered liquid phase is shown.

For this microscopic model, the existence of a finite region in which none of the homogeneous phases are linearly stable can now be rigorously proven. The hydrodynamic description indeed predicts that the disordered homogeneous phase  $\rho(x) = \rho_0$ ,  $m(x) = 0$  loses linear stability for densities such that  $\partial_m \tilde{F}(0, \rho) < 0$ , i.e.,  $\rho_0 > \rho_g^s \equiv \sinh(\beta)^{-1}$ . Then, a fully ordered solution appears given by  $\rho(x) = \rho_0$  and  $m_0$  the solution of

$$m_0 = \rho_0 \tanh[m_0 \sinh(\beta)]. \quad (20)$$

This solution is, however, linearly unstable for  $\rho_g^s < \rho_0 < \rho_\ell^s$  and leads to the traveling bands described above. At higher densities, for  $\rho_0 \geq \rho_\ell^s$ , the ordered uniform state becomes linearly stable. The corresponding phase diagram (Fig. 5) thus shows “spinodal curves”  $\rho_{g/\ell}^s(T)$  and “binodal curves”  $\rho_{g/\ell}(T)$ , in agreement with the liquid-gas scenario recently proposed for the flocking transition [27,46], for which the coexisting densities are such that  $\rho_g < \rho_g^s < \rho_\ell^s < \rho_\ell$ .

In this Letter, we have introduced lattice models for which one can derive exact hydrodynamic equations. Our strategy relies on scaling the rates of the different dynamical contributions so that they contribute equally at a diffusive hydrodynamic scale. The symmetric hopping, however, controls the dynamics at a local mesoscopic scale. This yields an explicit form for the local measure one needs to use to compute the average of any nonlinear function entering the dynamics of the mean local densities. Then, the hydrodynamic descriptions allow us to characterize the

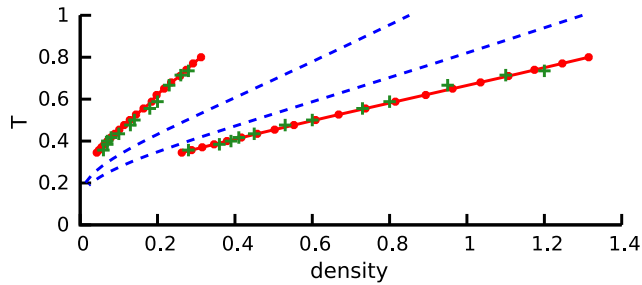


FIG. 5. Phase diagram of the flocking transition observed for dynamics 2.1–2.3 in the  $T, \rho$  plane for  $D = 0.5$  and  $\lambda = 1$ . The spinodals are shown in blue. Simulations of the hydrodynamics equations (red lines) and the microscopic model (green dots) lead to coexisting densities that are in agreement within the accuracy of our simulations.

large-scale emerging behaviors of these active lattice gases. In particular, we have introduced two models, presenting two of the most studied collective behaviors of active particles, namely, the motility-induced phase separation and the transition to collective motion. Constructing more general models is rather straightforward using the ingredients presented in this Letter [44], for instance, to study nematic alignment or the interplay between MIPS and aligning torques. Note that the hydrodynamic description is exact for finite macroscopic times in the  $L \rightarrow \infty$  limit. For large-but-finite sizes, describing the statistics of the active lattice-gas trajectories requires the addition of subleading fluctuating terms, in the spirit of the macroscopic fluctuation theory [18,55,56]. These terms are key to understanding the selection of metastable propagating solutions observed in simple flocking models [46,52,57]; their rigorous mathematical derivation, however, remains an open challenge.

We thank Alexandre Solon and Hugues Chaté for interesting discussions. J. T. and M. K. H. acknowledge support from the ANR Grant Bacterns. C. E. and T. B. acknowledge the support of ANR-15-CE40-0020-01 Grant LSD. C. E. is supported by the Brazilian National Council for Scientific and Technological Development (CNPq). Part of this work was done during the author's stay at the Institut Henri Poincaré–Centre Émile Borel during the trimester Stochastic Dynamics out of Equilibrium. The authors thank this institution for its support.

[1] M. Marchetti, J. Joanny, S. Ramaswamy, T. Liverpool, J. Prost, M. Rao, and R. A. Simha, *Rev. Mod. Phys.* **85**, 1143 (2013).  
 [2] P. Romanczuk, M. Bär, W. Ebeling, B. Lindner, and L. Schimansky-Geier, *Eur. Phys. J. Spec. Top.* **202**, 1 (2012).  
 [3] T. Vicsek and A. Zafeiris, *Phys. Rep.* **517**, 71 (2012).

[4] C. Bechinger, R. Di Leonardo, H. Löwen, C. Reichhardt, G. Volpe, and G. Volpe, *Rev. Mod. Phys.* **88**, 045006 (2016).  
 [5] T. Vicsek, A. Czirók, E. Ben-Jacob, I. Cohen, and O. Shochet, *Phys. Rev. Lett.* **75**, 1226 (1995).  
 [6] J. Toner and Y. Tu, *Phys. Rev. Lett.* **75**, 4326 (1995).  
 [7] V. Schaller, C. Weber, C. Semmrich, E. Frey, and A. R. Bausch, *Nature (London)* **467**, 73 (2010).  
 [8] A. Bricard, J.-B. Caussin, N. Desreumaux, O. Dauchot, and D. Bartolo, *Nature (London)* **503**, 95 (2013).  
 [9] H. H. Wensink, J. Dunkel, S. Heidenreich, K. Drescher, R. E. Goldstein, H. Löwen, and J. M. Yeomans, *Proc. Natl. Acad. Sci. U.S.A.* **109**, 14308 (2012).  
 [10] S. Ngo, A. Peshkov, I. S. Aranson, E. Bertin, F. Ginelli, and H. Chaté, *Phys. Rev. Lett.* **113**, 038302 (2014).  
 [11] M. E. Cates and J. Tailleur, *Annu. Rev. Condens. Matter Phys.* **6**, 219 (2015).  
 [12] I. Theurkauff, C. Cottin-Bizonne, J. Palacci, C. Ybert, and L. Bocquet, *Phys. Rev. Lett.* **108**, 268303 (2012).  
 [13] J. Palacci, S. Sacanna, A. P. Steinberg, D. J. Pine, and P. M. Chaikin, *Science* **339**, 936 (2013).  
 [14] E. Fodor, C. Nardini, M. E. Cates, J. Tailleur, P. Visco, and F. van Wijland, *Phys. Rev. Lett.* **117**, 038103 (2016).  
 [15] J. Tailleur and M. Cates, *Phys. Rev. Lett.* **100**, 218103 (2008).  
 [16] J. Tailleur and M. Cates, *Europhys. Lett.* **86**, 60002 (2009).  
 [17] G. Grégoire and H. Chaté, *Phys. Rev. Lett.* **92**, 025702 (2004).  
 [18] B. Derrida, *J. Stat. Mech.* (2007) P07023.  
 [19] E. Bertin, M. Droz, and G. Grégoire, *Phys. Rev. E* **74**, 022101 (2006).  
 [20] A. Ahmadi, M. C. Marchetti, and T. B. Liverpool, *Phys. Rev. E* **74**, 061913 (2006).  
 [21] E. Bertin, M. Droz, and G. Grégoire, *J. Phys. A* **42**, 445001 (2009).  
 [22] A. Baskaran and M. C. Marchetti, *Proc. Natl. Acad. Sci. U.S.A.* **106**, 15567 (2009).  
 [23] A. Baskaran and M. C. Marchetti, *J. Stat. Mech.* (2010) P04019.  
 [24] T. Ihle, *Phys. Rev. E* **83**, 030901 (2011).  
 [25] A. Peshkov, I. S. Aranson, E. Bertin, H. Chaté, and F. Ginelli, *Phys. Rev. Lett.* **109**, 268701 (2012).  
 [26] F. Thüroff, C. A. Weber, and E. Frey, *Phys. Rev. Lett.* **111**, 190601 (2013).  
 [27] A. Solon and J. Tailleur, *Phys. Rev. Lett.* **111**, 078101 (2013).  
 [28] E. Bertin, H. Chaté, F. Ginelli, S. Mishra, A. Peshkov, and S. Ramaswamy, *New J. Phys.* **15**, 085032 (2013).  
 [29] T. Ihle, *Eur. Phys. J. Spec. Top.* **223**, 1293 (2014).  
 [30] E. Bertin, A. Baskaran, H. Chaté, and M. C. Marchetti, *Phys. Rev. E* **92**, 042141 (2015).  
 [31] A. Manacorda and A. Puglisi, *Phys. Rev. Lett.* **119**, 208003 (2017).  
 [32] F. Bolley, J. A. Cañizo, and J. A. Carrillo, *Appl. Math. Lett.* **25**, 339 (2012).  
 [33] P. Degond and S. Motsch, *Math. Models Methods Appl. Sci.* **18**, 1193 (2008).  
 [34] A. Czirók, H. E. Stanley, and T. Vicsek, *J. Phys. A* **30**, 1375 (1997).  
 [35] O. O'Loan and M. Evans, *J. Phys. A* **32**, L99 (1999).

- [36] F. Peruani, T. Klaus, A. Deutsch, and A. Voss-Boehme, *Phys. Rev. Lett.* **106**, 128101 (2011).
- [37] A. Thompson, J. Tailleur, M. Cates, and R. Blythe, *J. Stat. Mech.* (2011) P02029.
- [38] R. Soto and R. Golestanian, *Phys. Rev. E* **89**, 012706 (2014).
- [39] K. R. Pilkievicz and J. D. Eaves, *Phys. Rev. E* **89**, 012718 (2014).
- [40] S. Whitelam, K. Klymko, and D. Mandal, *J. Chem. Phys.* **148**, 154902 (2018).
- [41] A. De Masi, P. Ferrari, and J. Lebowitz, *Phys. Rev. Lett.* **55**, 1947 (1985).
- [42] G. Jona-Lasinio, C. Landim, and M. Vares, *Probab. Theory Relat. Fields* **97**, 339 (1993).
- [43] T. Bodineau and M. Lagouge, *J. Stat. Phys.* **139**, 201 (2010).
- [44] C. Erignoux, [arXiv:1608.04937](https://arxiv.org/abs/1608.04937).
- [45] Y. Fily and M. C. Marchetti, *Phys. Rev. Lett.* **108**, 235702 (2012).
- [46] A. P. Solon, H. Chaté, and J. Tailleur, *Phys. Rev. Lett.* **114**, 068101 (2015).
- [47] Note that the coarse-grained dynamics of  $\rho^\pm$  would be the same for any choice of  $\delta$ .
- [48] H. Spohn, *Large-Scale Dynamics of Interacting Particles* (Springer Science+Business Media, New York, 2012).
- [49] This is despite the fact that there is a single conserved quantity.
- [50] M. Clincy, B. Derrida, and M. R. Evans, *Phys. Rev. E* **67**, 066115 (2003).
- [51] R. A. Blythe and M. R. Evans, *J. Phys. A* **40**, R333 (2007).
- [52] A. P. Solon, J.-B. Caussin, D. Bartolo, H. Chaté, and J. Tailleur, *Phys. Rev. E* **92**, 062111 (2015).
- [53] A. P. Solon, J. Stenhammar, M. E. Cates, Y. Kafri, and J. Tailleur, *Phys. Rev. E* **97**, 020602 (2018).
- [54] A. P. Solon, J. Stenhammar, M. E. Cates, Y. Kafri, and J. Tailleur, [arXiv:1803.06159](https://arxiv.org/abs/1803.06159).
- [55] L. Bertini, A. De Sole, D. Gabrielli, G. Jona-Lasinio, and C. Landim, *J. Stat. Phys.* **107**, 635 (2002).
- [56] J. Tailleur, J. Kurchan, and V. Lecomte, *J. Phys. A* **41**, 505001 (2008).
- [57] J.-B. Caussin, A. Solon, A. Peshkov, H. Chaté, T. Dauxois, J. Tailleur, V. Vitelli, and D. Bartolo, *Phys. Rev. Lett.* **112**, 148102 (2014).